J. Fluid Mech. (1983), *vol.* 135, *pp.* 407–434
Printed in Great Britain

Universality and strange attractors in internal-wave dynamics

By HENRY D. I. ABARBANEL†
Lawrence Berkeley Laboratory, University of California, Berkeley, CA 94720

(Received 26 March 1983 and in revised form 21 June 1983)

We argue that the universality and statistical nature of the deep-ocean internal gravity-wave spectrum results from a strange attractor in the driven, dissipative internal-wave field. To explore this we construct a model which injects energy into the oceanic surface at a constant rate. A two-dimensional version of the model is explored analytically and numerically. For the numerical work we restrict our considerations to a few of the longest-wavelength modes. This few-mode system exhibits bifurcation into limit cycles, period doubling of the limit cycles, and chaotic, non-periodic behaviour associated with a strange attractor. In an appendix we present some discussion of the three-dimensional version of the model.

1. Introduction

The universality of the empirical oceanic internal-wave spectrum (Garrett & Munk 1975, 1979) is a striking feature of internal-wave dynamics. Since the sources for energy influx into the internal-wave field (Thorpe 1975) are numerous and irregularly placed in time as well as space, it appears unlikely that a study of sources, however much they may reveal about ocean dynamics (Wunsch 1975), will illuminate the universality question.

Various mechanisms of energy dissipation and energy redistribution have been reviewed critically by Holloway (1980). He concludes that wave–wave interactions are not weak and that no firm clues to the origin of the universal spectrum have been uncovered.

In this article we begin the exploration of another path which leads to universal behaviour in dynamical systems like oceanic internal waves. We begin with the observation that the response of the internal-wave system (in the deep ocean) to changes in energy sources is at most a transient which is lost as the system settles back to its universal state. Secondly, we note that, although much of the internal-wave field dissipates negligible energy, the energy input by sources must, of course, be dissipated by fluid motions on scales < 5 m.

Viewing a change in energy sources as equivalent to a change in 'initial' conditions, we see that the asymptotic state to which the internal-wave field goes is rather independent of initial conditions. Dissipative systems which approach the same state for a large set of initial conditions are said to have an *asymptotic attractor* or invariant distribution (Eckmann 1981). The motion of a given phase-space point (internal-wave field Fourier mode in the present context) will be quite complicated on the attractor. Indeed the details of the orbit will be very sensitive to initial conditions. The distribution of points on the attractor, however, is the same for all initial points in its basin of attraction.

† Present address: University of California, San Diego, MPL, A-005, La Jolla, CA 92093.

The path we wish to begin pursuing here rests on the notion that internal-wave dynamics has an asymptotic attractor with a wide basin of attraction, so that a large variety of initial or perturbed states of the ocean relaxes rather rapidly to this universal asymptotic state. If we have N modes of the internal-wave field of dynamic importance, the state of the system is labelled at any time by an N-vector $\boldsymbol{x} = (x_1, x_2, \ldots, x_N)$. If we know $D_A(\boldsymbol{x})$ – the asymptotic distribution – then the distribution of any phase function $F(\boldsymbol{x})$, such as the energy, is $F(\boldsymbol{x})\, D_A(\boldsymbol{x})$ when the asymptotic state is reached.

Until now we have been addressing properties of the *deterministic* evolution equations which govern the internal-wave field. Yet it is an aspect of the empirical data that it is appropriate to treat internal-wave motion as *statistical*. These two views are joined when we inquire into the structures available for $D_A(\boldsymbol{x})$. Since the system is dissipative, any volume of phase space shrinks to zero in going from the initial state to the asymptotic state. We can state this differently by saying that the attractor has dimension $< N$, so has phase-space *volume* zero.

The simplest possible attractor is a fixed point, which has dimension zero. As the parameters of the system (magnitude of surface wind stress, strength of mean currents, etc.) change, so may the topology of the attractor. The next most complicated attractor is a limit cycle in which orbits settle down to a closed curve in $\boldsymbol{x}$-space. These have dimension one. Motion on a torus in $M < N$ dimensions is the natural generalization of the limit cycle; such flows have dimension M and are *quasi-periodic*. About a decade ago it was pointed out (Ruelle & Takens 1971) that there is another possibility for the topology of the attractor. It is possible that, after several (3 or 4) bifurcations from limit cycles, the attractor will become *non-periodic*. The asymptotic orbit will not be a closed curve in $\boldsymbol{x}$-space, but will fill some number of integer dimensions plus a Cantor set of points with *fractional dimension*. This is aptly called a *strange attractor*. (Good introductory expositions of this idea are in Lanford (1980) and Ott (1981).) Such behaviour had been observed in earlier work by Lorenz (1963) in the context of Bénard convection. Also there is rather clean experimental evidence that this route to non-periodic motion does occur (Fenstermacher, Swinney & Gollub 1979; Libchaber & Maurer 1981).

When non-periodic motion on a strange attractor does set in, a spectral analysis of the orbit will reveal only broadband structure and no sharp lines from periodic or quasi-periodic motion. Since the motion is non-periodic it may properly be termed *chaotic* or *turbulent*, though it is clear it cannot correctly be called stochastic, statistical, or random in the strictest sense of those terms. If one subjects orbits on a strange attractor to tests for a random function of time, it will pass them to high numerical resolution. One may then call the motion pseudorandom, and in an operational sense treat it as statistical.

In this paper we study a model of forced internal-wave dynamics in which the energy sources are taken to be at the oceanic surface and are represented by a phenomenological scalar field, $E(\boldsymbol{x}, t)$, which we term the *energy-transfer field*. It is taken to satisfy an advection diffusion equation

$$\left(\frac{\partial}{\partial t} + \boldsymbol{u} \cdot \boldsymbol{\nabla}_x\right) E(\boldsymbol{x}, t) = \kappa \nabla^2 E(\boldsymbol{x}, t),$$

where $\boldsymbol{u}(\boldsymbol{x}, t)$ is the fluid velocity field and κ is a phenomenological energy diffusivity. The energy-transfer field also will couple into the Navier–Stokes equation for $\boldsymbol{u}$. Energy input will be represented by a fixed value of E, call it E_0, at the ocean surface

and a zero value at the ocean bottom. As E_0 is varied the internal-wave field is more or less strongly driven from one asymptotic state to another. We wish to examine the variety of asymptotic states available to the stratified fluid.

In a loose way one can think of our model as an inverse sort of convection problem; namely, we have a stratified fluid 'heated' from above. Such a situation is not subject to convective instability as occurs in ordinary Bénard convection, but instead is prone to the Kelvin–Helmholtz instability (Chandrasekhar 1961; Bretherton 1969) which occurs as the fluid is driven to strong vertical shears which overcome the stability of buoyancy effects due to the stratification. When the quantity

$$\mu = \frac{\partial u_x}{\partial z}\Big/ n,$$

where n is the buoyancy frequency, u_x is the x-component of $\boldsymbol{u}$, and the stratification is in the z-direction, becomes greater than 2, one expects instability. The conventional Richardson number is μ^{-2}, and there is quite striking evidence that internal-wave modes with $\mu > 2$ ($Ri < \frac{1}{4}$) are absent in the oceanic internal-wave field (Eriksen 1978). In our scaling of the dynamical equations μ will become a measure of the strength with which the energy-transfer field couples to the velocity and density fields and the nonlinear coupling strength of modes of the linear system. It is the instabilities of dynamical systems which allow the topology of strange attractors to emerge, so our study here will focus on the qualitative features of the internal-wave field as μ varies.

Our eventual model is, of course, an abstraction even of the simplified situation of 'heating' which we have described above. The three most bold approximations we make are (1) the buoyancy frequency is taken constant; (2) the ocean is taken to be two-dimensional – one horizontal direction is suppressed; (3) we make a mode expansion of the full partial differential equations to reduce them to a few ordinary differential equations. Our physical idea here is that for small, but non-trivial, forcing the longest-wavelength modes will both be more dominant and more prone to instability. Small-wavelength modes are also damped more strongly by viscosity. All of our approximations are open to examination by removing them. Variable $n(z)$ complicates the algebra and changes the details of mode couplings. Three space dimensions instead of two can be handled, but we do not examine this difference in our initial exploration here. Finally one can always augment the number of modes retained.

In §2 we discuss our model in more detail. We exhibit the scalings used and derive the modal equations. In §3 we study the simplest mode truncation of our system. It involves 5 modes. The five-mode system shows all the features of bifurcation to limit cycles and strange attractors indicated before. Our numerical work indicates that the route to chaos taken by the five-mode system could well be that of period doubling, which is not uncommon for low-order systems of ordinary differential equations. However, both in response to questions raised by one of the referees and the very helpful suggestions of E. Ott and C. Grebogi, I wish to draw the readers' attention to the papers of Kuramoto & Koga (1982) and of Lyubimov & Zaks (1983) in which it is noted that chaos can result from a sequence of 'repeated splitting(s) and recombination(s) of closed orbits'. The qualitative features of the phase portraits and return maps in these papers are much like those in the present work. We have not been able to verify that the phenomena seen by these authors is what we are observing here. The most straightforward interpretation of our results from a dynamical-systems point of view is that we are seeing period doubling. The various

power spectra we present strongly support this. In all there is here a bit of a puzzle, which is not resolved in the present work, but certainly deserves contemplation.

Most of the work presented here is numerical, though some of the analysis of the instability of the fixed point in its transition to a limit cycle is analytic and is used as a quantitative support of the features of our numerical solutions. We present orbits and power spectra for an interesting range of μ. Section 4 contains a discussion of the work in the paper and indications of future routes to investigate.

2. Model of a forced stratified fluid

Our starting point is the usual Boussinesq approximation (Chandrasekhar 1961; Phillips 1977) for coupled velocity $\boldsymbol{u}(\boldsymbol{x},t)$ and density $\rho(\boldsymbol{x},t)$ fields:

$$\frac{\partial}{\partial t}\boldsymbol{u}+(\boldsymbol{u}\cdot\boldsymbol{\nabla})\boldsymbol{u}=-\frac{1}{\rho_0}\boldsymbol{\nabla}p-\frac{\rho g}{\rho_0}\hat{\boldsymbol{z}}+\boldsymbol{u}\times\boldsymbol{f}+\nu\nabla^2\boldsymbol{u}, \tag{1}$$

$$\operatorname{div}\boldsymbol{u}=0, \tag{2}$$

$$\frac{\partial}{\partial t}\rho_1+(\boldsymbol{u}\cdot\boldsymbol{\nabla})\rho_1-\frac{\rho_0}{g}n^2(x_3)\,u_3=0, \tag{3}$$

where $\rho=\rho(x_3)+\rho_1(\boldsymbol{x},t)$, $n(x_3)$ is the usual buoyancy frequency, p is the pressure, g the gravitational acceleration, $\hat{\boldsymbol{z}}$ a unit vector in the 3-direction (taken upward), $\boldsymbol{f}$ the Coriolis parameter ($\boldsymbol{f}=f\hat{\boldsymbol{z}}, f=2\omega_{\text{inertial}}\sin(\text{latitude})$), and ν is the kinematic viscosity.

To these familiar equations we wish to add an energy source which will drive the motion of internal waves. We accomplish this by introducing a scalar *energy-transfer field* $E(\boldsymbol{x},t)$, which is taken to provide a force in the 3-direction in the momentum equation (1) and satisfy its own advection–diffusion equation

$$\left(\frac{\partial}{\partial t}+\boldsymbol{u}\cdot\boldsymbol{\nabla}\right)E(\boldsymbol{x},t)=\kappa\nabla^2E(x,t), \tag{4}$$

where κ is the phenomenological rate at which the energy-transfer amplitude is dissipated.

In the momentum equation we add to the right-hand side a forcing term

$$-\beta\hat{\boldsymbol{z}}E(\boldsymbol{x},t), \tag{5}$$

where β is another phenomenological parameter but of no real significance as it can be scaled away since (4) is homogeneous in $E(\boldsymbol{x},t)$. This term is supposed to represent the result of a more detailed calculation of the way energy is transferred into the oceanic depths by surface mechanisms. A model calculation of this sort is the work of Watson, West & Cohen (1976), and such a calculation would yield a value for β.

One of the referees has quite properly raised the issue of the relation of the model we have set up in (1)–(4) to the more conventional formulation as found, for example, in the monograph of Pedlosky (1979). The particular difference is in the 'energy' equation (4), which is usually replaced by a 'density diffusion'. Pedlosky notes that this is just the heat or energy equation with a particular linear relationship between the temperature and the density. Here, in the internal-wave problem, density is a dynamical degree of freedom satisfying its own advective evolution equation (3). Our field $E(\boldsymbol{x},t)$ is really no more than a representation of the heat equation without the identification of E with temperature, and the subsequent statement of an equation of state connecting density with temperature. With the three equations (1)–(3) we

have five evolution equations for five fields (three velocity, one density and one pressure). In themselves they are now closed. In order to drive this dissipative system, we must put energy in either through boundary conditions, say on the velocity at the surface, or though another field, as we have done. A more realistic model would have the internal-wave field driven, say, by shears in the large-scale quasi-geostrophic flow. We will explore such complicated models in future work, but have chosen to remain with the simplistic replacement of the usual energy equation to bring out the other issues raised in this paper.

We require the field $E(\boldsymbol{x}, t)$ to be a fixed constant value E_0 at the surface, $x_3 = 0$, and zero at the bottom $x_3 = -D$. This represents energy forcing at the surface. Just as we may split $\rho(\boldsymbol{x}, t)$ into the background stratification $\bar{\rho}(x_3)$ and the density variations $\rho_1(\boldsymbol{x}, t)$, so we may split $E(\boldsymbol{x}, t)$ as:

$$E(\boldsymbol{x}, t) = E_0(1 + x_3/D) + E_1(\boldsymbol{x}, t), \tag{6}$$

where the first term satisfies the surface and bottom boundary conditions, as well as the linearized version of our equations, while $E(\boldsymbol{x}, t)$ is the energy-transfer variation about the energy conduction $E_0(1 + x_3/D)$.

A discussion of the three-dimensional version of our model will be found in the appendix. Here we restrict ourselves to two dimensions (x_1, x_3). Introduce a stream function $\psi(x_1, x_3, t)$ in the usual fashion

$$u_1 = \frac{\partial \psi}{\partial x_3}, \quad u_3 = -\frac{\partial \psi}{\partial x_1} \tag{7}$$

to guarantee

$$\operatorname{div} \boldsymbol{u} = 0. \tag{8}$$

The equations of motion for the three independent fields $\nabla^2\psi$, E_1 and ρ_1 are derived from (1), (3) and (4):

$$\left(\frac{\partial}{\partial t} - \nu\nabla^2\right)\nabla^2\psi = \frac{\partial}{\partial x_1}\left(\frac{g\rho_1}{\rho_0} + \beta E_1\right) + \mathrm{J}(\psi, \nabla^2\psi), \tag{9}$$

$$\frac{\partial}{\partial t}\rho_1 + \frac{n^2\rho_0}{g}\frac{\partial \psi}{\partial x_1} + \mathrm{J}(\psi, \rho_1) = 0, \tag{10}$$

$$\left(\frac{\partial}{\partial t} - \kappa\nabla^2\right)E_1 + \mathrm{J}(\psi, E_1) = \frac{E_0}{D}\frac{\partial \psi}{\partial x_1}, \tag{11}$$

where

$$\mathrm{J}(f, g) = \frac{\partial f}{\partial x_3}\frac{\partial g}{\partial x_1} - \frac{\partial f}{\partial x_1}\frac{\partial g}{\partial x_3}. \tag{12}$$

We now turn our attention to a constant-n ocean, so the natural timescale is n^{-1}. The natural lengthscale is D; so we are ignoring lengthscales for the variation of n. With these dimensional quantities we scale our equations by the rules

$$t \to t/n, \tag{13}$$

$$\psi \to \mu n D^2 \psi, \tag{14}$$

$$E_1 \to E_0 E_1, \tag{15}$$

$$\rho_1 \to \frac{\rho_0 n^2 D\mu}{g}\rho_1, \tag{16}$$

$$(x_1, x_3) \to D(x, z). \tag{17}$$

The momentum equation suggests that the choice

$$\beta E_0 = n^2 D\mu \tag{18}$$

is consistent with the interpretation of μ as the ratio of horizontal velocity shear to buoyancy frequency. These scalings yield

$$\frac{\partial}{\partial t}\nabla^2\psi - \Gamma_1\nabla^4\psi = \frac{\partial}{\partial x}(\rho_1 + E_1) + \mu \mathrm{J}(\psi, \nabla^2\psi), \tag{19}$$

$$\frac{\partial}{\partial t}\rho_1 + \frac{\partial\psi}{\partial x} + \mu \mathrm{J}(\psi, \rho_1) = 0, \tag{20}$$

$$\left(\frac{\partial}{\partial t} - \Gamma_2\nabla^2\right)E_1 + \mu \mathrm{J}(\psi, E_1) = \mu\frac{\partial\psi}{\partial x}, \tag{21}$$

where $\Gamma_1 = \nu/hD^2$ and $\Gamma_2 = \kappa/nD^2$. The role of μ as the strength of the nonlinearities is made explicit by these rescalings.

The trivial solution to (19)–(21), $\psi = \rho_1 = E_1 = 0$, represents the background state where the density is $\bar{\rho}$, energy is conducted from the surface into the ocean, and there is no fluid motion. To study the stability of this state we take the fields to be in a particular Fourier mode

$$\psi(x, z, t) = \psi \sin \pi q z \sin\frac{\pi m x}{L} e^{\lambda t}, \tag{22}$$

$$\rho_1(x, z, t) = \rho_1 \sin \pi q z \cos\frac{\pi m x}{L} e^{\lambda t}, \tag{23}$$

$$E_1(x, z, t) = E_1 \sin \pi q z \cos\frac{\pi m x}{L} e^{\lambda t}. \tag{24}$$

The particular choice of sines and cosines comes from the boundary conditions $u_3 = \rho_1 = E_1 = 0$ at $z = 0, -1$ and $u_1 = 0$ at the sides of the ocean, taken to be at $x = \pm L$.

The linear terms of (19)–(21) lead to

$$\begin{bmatrix} -k_{qm}^2(\lambda + \Gamma_1 k_{qm}^2) & k_x & k_x \\ k_x & \lambda & 0 \\ -\mu k_x & 0 & \lambda + \Gamma_2 k_{qm}^2 \end{bmatrix} \begin{bmatrix} \psi \\ \rho_1 \\ E_1 \end{bmatrix} = 0, \tag{25}$$

where

$$k_x = \frac{\pi m}{L}, \quad k_{qm}^2 = \pi^2\left(q^2 + \frac{m^2}{L^2}\right). \tag{26}$$

To have non-zero amplitudes we require

$$k_{qm}^2\lambda^3 + \lambda^2 k_{qm}^4(\Gamma_1 + \Gamma_2) + \lambda(\Gamma_1\Gamma_2 k_{qm}^6 + k_x^2(1-\mu)) + \Gamma_2 k_{qm}^2 k_x^2 = 0, \tag{27}$$

and the variations about $\psi = \rho_1 = E_1 = 0$ are stable when (27) has no roots with positive real part.

This equation for λ has one real negative solution as long as $\Gamma_2 k_{qm}^2 k_x^2 > 0$. Assuming that to be true, we seek a solution with $\mathrm{Re}\,\lambda_0 = 0$. This occurs when

$$(\mathrm{Im}\,\lambda_0)^2 = \frac{\Gamma_2 k_x^2}{k_{qm}^2(\Gamma_1 + \Gamma_2)} = \frac{k_{qm}^6\Gamma_1\Gamma_2 + k_x^2(1-\mu)}{k_{qm}^2}. \tag{28}$$

The other solution of (27) is $-k_{qm}^2(\Gamma_1+\Gamma_2)$ at this point; namely, that eigenmotion is stable. By writing $\lambda = \mathrm{i}\,\mathrm{Im}\,\lambda_0+\delta$, we find that $\delta < 0$, than is the $\psi = \rho_1 = E_1 = 0$ solution is stable, when

$$\mu < \mu_c(q,m) = \frac{\Gamma_1}{\Gamma_1+\Gamma_2}+\Gamma_1\Gamma_2\frac{(q^2+m^2/L^2)^3\pi^4L^2}{m^2}, \tag{29}$$

and unstable for $\mu > \mu_c(q,m)$. In other words, if we set μ, Γ_1 and Γ_2, then all modes with horizontal wavenumber $\pi m/L$ and vertical wavenumber πq such that $\mu_c(q,m) < \mu$ are unstable.

This instability is that of the standard Hopf bifurcation (Iooss & Joseph 1981), where a complex-conjugate pair of eigenvalues of a linear stability matrix cross the imaginary axis. Whether a limit cycle emerges as these eigenvalues acquire a positive real part depends in detail on the structure of the nonlinearities. The numerical work presented below indicates that a normal Hopf bifurcation occurs at μ_c and that a limit cycle of amplitude $(\mu-\mu_c)^{\frac{1}{2}}$ grows out of the fixed point. At μ_c the frequency of the limit-cycle oscillations is

$$\left(\frac{\Gamma_2}{\Gamma_1+\Gamma_2}\right)^{\frac{1}{2}}\Omega(q,m), \tag{30}$$

where

$$\Omega(q,m)^2 = \frac{k_x^2}{k_{qm}^2} \tag{31}$$

$$= \frac{m^2}{q^2L^2+m^2}, \tag{32}$$

which is the frequency of the familiar linear internal-wave eigenmode measured in time units scaled by n.

The form of $\mu_c(q,m)$ in (29) shows that, as μ increases beyond μ_c, modes become unstable one at a time and that it is the low-q, low-m modes which are most prone to instability. So we observe that it is the longest-wavelength modes which first contribute to interesting structure as the internal-wave field is driven more and more strongly. This suggests that, for moderate values of μ, a few-mode approximation to the full partial differential equations will provide a good qualitative understanding of the behaviour of the full system. As μ becomes larger, more and more modes become important.

We turn now to a few-mode approximation to the two-dimensional internal-wave equations. Expand ψ, ρ_1 and E_1 in eigenmodes as

$$\begin{Bmatrix}\psi(x,z,t)\\ \rho_1(x,z,t)\\ E_1(x,z,t\end{Bmatrix} = \sum_{q,\,m=-\infty}^{+\infty} \mathrm{e}^{\mathrm{i}q\pi z+\mathrm{i}m\pi x/L}\begin{Bmatrix}\phi_{qm}(t)\\ \mathrm{i}\rho_{qm}(t)\\ \mathrm{i}\epsilon_{qm}(t)\end{Bmatrix}. \tag{33}$$

The boundary conditions at $z = 0$, -1 and $x = \pm L$ along with the reality of ψ, ρ_1 and E_1 result in the conditions

$$\phi_{q,m}^* = \phi_{-q,-m}, \quad \phi_{q,m} = -\phi_{-q,m} = -\phi_{q,-m}, \tag{34}$$

$$(\rho,\epsilon)_{q,m}^* = -(\rho,\epsilon)_{-q,-m}, \quad (\rho,\epsilon)_{q,m} = -(\rho,\epsilon)_{-q,m} = (\rho,\epsilon)_{q,-m}. \tag{35}$$

From the partial differential equations for ψ, ρ_1 and E_1 we derive the coupled ordinary differential equations for the modal amplitudes:

$$-k_{qm}^2\left[\frac{\mathrm{d}\phi_{qm}}{\mathrm{d}t}+\Gamma_1 k_{qm}^2\phi_{qm}\right]+\frac{\pi m}{L}(\rho_{qm}+\epsilon_{qm}) = \frac{\mu\pi^2}{L}\sum_{q_1 m_1} k_{q_1 m_1}\phi_{q_1 m_1}\phi_{q-q_1,\, m-m_1}(m_1 q-q_1 m), \quad (36)$$

$$\frac{\mathrm{d}}{\mathrm{d}t}\rho_{qm}+\frac{\pi m}{L}\phi_{qm} = \frac{\mu\pi^2}{L}\sum_{q_1,\, m_1}\rho_{q_1 m_1}\phi_{q-q_1,\, m-m_1}(m_1 q-q_1 m), \quad (37)$$

$$\left[\frac{\mathrm{d}}{\mathrm{d}t}+\Gamma_2 k_{qm}^2\right]\epsilon_{qm}-\frac{\mu\pi m}{L}\phi_{qm} = \frac{\mu\pi^2}{L}\sum_{q_1,\, m_1}\epsilon_{q_1 m_1}\phi_{q-q_1,\, m-m_1}(m_1 q-q_1 m). \quad (38)$$

This infinite set of coupled equations is equivalent to the original equations for ψ, ρ_1 and E_1. We proceed by retaining only a few modes with small wavenumbers. In addition to the linear stability argument given above we have two arguments for this. (1) For some range of driving strength μ only the lowest-wavenumber modes will be substantially excited; higher wavenumbers require larger kinetic energy. (2) Since dissipation is proportional to $\Gamma_1 k_{q,m}^2$, modes with larger wavenumbers will be more rapidly destroyed. So the energy in larger k_{qm} will not have had time to circulate before it disappears into a dissipative sink. As μ increases, more modes will become required for an accurate description of the system.

In the remainder of this paper we deal with the baldest truncation of our coupled equations. The smallest-wavenumber modes that give rise to nonlinear coupling are five: ϕ_{11}, ρ_{11}, ϵ_{11} and ρ_{20} and ϵ_{20}. ϕ_{10} and ϕ_{01} are identically zero by (32), as are ρ_{01} and ϵ_{01}. The modes ϵ_{10} and ρ_{10} are constants to this order. Our five-mode system satisfies

$$-k_{11}^2\frac{\mathrm{d}\phi_{11}}{\mathrm{d}t}-\Gamma_1 k_{11}^2\phi_{11}+\frac{\pi}{L}(\rho_{11}+\epsilon_{11}) = 0, \quad (39)$$

$$\frac{\mathrm{d}}{\mathrm{d}t}\rho_{11}+\frac{\pi}{L}\phi_{11} = \frac{2\mu\pi^2}{L}\rho_{20}\phi_{11}, \quad (40)$$

$$\frac{\mathrm{d}}{\mathrm{d}t}\rho_{20} = -\frac{4\mu\pi^2}{L}\rho_{11}\phi_{11}, \quad (41)$$

$$\frac{\mathrm{d}}{\mathrm{d}t}\epsilon_{11}+\Gamma_2 k_{11}^2\epsilon_{11}-\frac{\mu\pi}{L}\phi_{11} = \frac{2\mu\pi^2}{L}\epsilon_{20}\phi_{11}, \quad (42)$$

$$\frac{\mathrm{d}}{\mathrm{d}t}\epsilon_{20}+\Gamma_2 k_{20}^2\epsilon_{20} = -\frac{4\mu\pi^2}{L}\epsilon_{11}\phi_{11}. \quad (43)$$

3. Analysis of the five-mode system

We begin with the equations for ρ_{20} and ρ_{11}:

$$\frac{\mathrm{d}}{\mathrm{d}t}\rho_{11}+\frac{\pi}{L}\phi_{11} = \frac{2\mu\pi^2}{L}\rho_{20}\phi_{11},$$

$$\frac{\mathrm{d}}{\mathrm{d}t}\rho_{20} = -\frac{4\mu\pi^2}{L}\rho_{11}\phi_{11}.$$

By making the change of variables

$$\rho_{20}\to\sqrt{2}\,\rho_{20}+\frac{1}{2\pi\mu}, \quad \rho_{11}\to\rho_{11}, \quad (44)$$

we find

$$\frac{\mathrm{d}}{\mathrm{d}t}\rho_{20} = -\frac{\sqrt{2}\,2\mu\pi^2}{L}\rho_{11}\phi_{11}, \tag{45}$$

$$\frac{\mathrm{d}}{\mathrm{d}t}\rho_{11} = +\frac{\sqrt{2}\,2\mu\pi^2}{L}\rho_{20}\phi_{11}, \tag{46}$$

which means

$$\rho_{11}^2+\rho_{20}^2 = \tilde{R}^2 = \text{constant}; \tag{47}$$

so we write

$$\rho_{11} = -\tilde{R}\sin\theta, \quad \rho_{20} = -\tilde{R}\cos\theta, \tag{48}$$

which leads to

$$\frac{\mathrm{d}}{\mathrm{d}t}\phi_{11}+\alpha\phi_{11} = \frac{\pi}{k_{11}^2 L}(\epsilon_{11}-\tilde{R}\sin\theta), \tag{49}$$

$$\frac{\mathrm{d}}{\mathrm{d}t}\epsilon_{11}+\gamma\epsilon_{11}-\frac{\pi\mu}{L}\phi_{11} = \frac{2\mu\pi^2}{L}\epsilon_{20}\phi_{11}, \tag{50}$$

$$\frac{\mathrm{d}}{\mathrm{d}t}\epsilon_{20}+\gamma^1\epsilon_{20} = -\frac{4\mu\pi^2}{L}\epsilon_{11}\phi_{11}, \tag{51}$$

$$\frac{\mathrm{d}}{\mathrm{d}t}\theta = \frac{2\sqrt{2}\,\mu\pi^2}{L}\phi_{11}, \tag{52}$$

where $\alpha = \Gamma_1 k_{11}^2$, $\gamma = \Gamma_2 k_{11}^2$ and $\gamma^1 = \Gamma_2 k_{20}^2$. By making the rescalings

$$\phi_{11} = \frac{L\alpha}{2\sqrt{2}\,\pi^2\mu}\Phi, \tag{53}$$

$$\epsilon_{11} = \frac{k_{11}^2 L^2\alpha^2}{2\sqrt{2}\,\pi^3\mu}E_{11}, \tag{54}$$

$$\epsilon_{20} = \frac{k_{11}^2 L^2\alpha^2}{2\pi^3\mu}E_{20}, \tag{55}$$

$$\tilde{R} = \frac{k_{11}^2 L^2\alpha^2}{2\sqrt{2}\,\pi^3\mu}R, \tag{56}$$

$$t = s/\alpha, \tag{57}$$

we may cast our equations into the more manageable form

$$\frac{\mathrm{d}\Phi}{\mathrm{d}s} = -\Phi+E_{11}-R\sin\theta, \tag{58}$$

$$\frac{\mathrm{d}}{\mathrm{d}s}E_{11} = -\frac{\gamma}{\alpha}E_{11}+\left[\frac{\mu^2}{\alpha^2}\Omega^2+E_{20}\right]\Phi, \tag{59}$$

$$\frac{\mathrm{d}}{\mathrm{d}s}E_{20} = \frac{\gamma^1}{\alpha}E_{20}-E_{11}\Phi, \tag{60}$$

$$\frac{\mathrm{d}\theta}{\mathrm{d}s} = \Phi, \tag{61}$$

where

$$\Omega^2 = \pi^2/k_{11}^2 L^2 \tag{62}$$

is the eigenfrequency of the $q = m = 1$ linear internal-wave eigenmode.

The rate of contraction of phase-space volumes is given by (Arnol'd 1978)

$$\frac{\partial\dot{\Phi}}{\partial\Phi}+\frac{\partial\dot{E}}{\partial E_{11}}+\frac{\partial\dot{E}_{20}}{\partial E_{20}}+\frac{\partial\dot{\theta}}{\partial\theta} = -\left[1+\frac{\gamma^1}{\alpha}+\frac{\gamma}{\alpha}\right]. \tag{63}$$

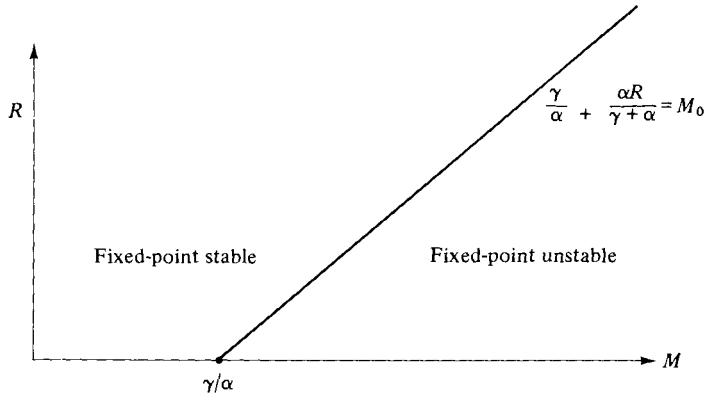

FIGURE 1. Region of stability of the fixed point $\Phi = E_{11} = E_{20} = \theta = 0$. For $M < M_0 = \gamma/\alpha + \alpha R/(\gamma+\alpha)$ the fixed point is stable. For $M < M_0$ the fixed point bifurcates into a limit cycle. With our choice of parameters $\gamma = \alpha$ and $R = 1.0$, so $M_0 = 1.5$.

Since this is constant over state space, a volume $V(0)$ becomes

$$V(s) = V(0)\exp[-s(1+\gamma/\alpha+\gamma^1/\alpha)]$$

as 'time' goes by.

These equations have one fixed point at $\Phi = E_{11} = E_{20} = \theta = 0$. This corresponds to no motion of the velocity or energy-transfer fields and a constant value for the $q = 2$, $m = 0$ piece of the density. The stability of this fixed point is governed by the eigenvalues of the linear stability matrix. If variations about the fixed point behave as $e^{s\lambda}$, then stability is determined by the values of λ satisfying

$$\left(\lambda+\frac{\gamma^1}{\alpha}\right)\left[\lambda^3+\lambda^2\left(1+\frac{\gamma}{\alpha}\right)+\lambda\left(\frac{\gamma}{\alpha}-M+R\right)+\frac{R\gamma}{\alpha}\right] = 0, \tag{64}$$

where

$$M = \mu\Omega^2/\alpha^2. \tag{65}$$

The root at $\lambda = -\gamma^1/\alpha$ is always stable. If $R\gamma/\alpha > 0$, there is always another negative real root. The other roots are complex conjugates and have zero real part when $\lambda = i\sigma$. This requires

$$\sigma^2 = \frac{\gamma R}{\gamma+\alpha}, \tag{66}$$

and occurs when

$$M = M_0 = \frac{\gamma}{\alpha}+\frac{\alpha R}{\gamma+\alpha}. \tag{67}$$

When $M > M_0$, the roots acquire a positive real part and the fixed point is unstable (see figure 1).

The instability is of the classical Hopf-bifurcation variety (Ioos & Joseph 1981). It is possible to determine analytically whether the bifurcation is 'normal', so a limit cycle grows smoothly out of the fixed point, or 'inverted', so an unstable limit cycle absorbs the newborn limit cycle and the whole set-up moves on to another behaviour. The numerical work soon to be discussed shows that, at least in the region of the parameter space we have explored, a normal Hopf bifurcation occurs.

Now we turn to the numerical calculations we have carried out on the system (49)–(52). In all the work we present here we choose $\gamma = \gamma^1 = \alpha$ and $R = 1.0$. For other values of these parameters the *qualitative* features of the motion are the same. With these values the fixed point becomes unstable at $M_0 = \frac{3}{2}$. In figure 2 we present

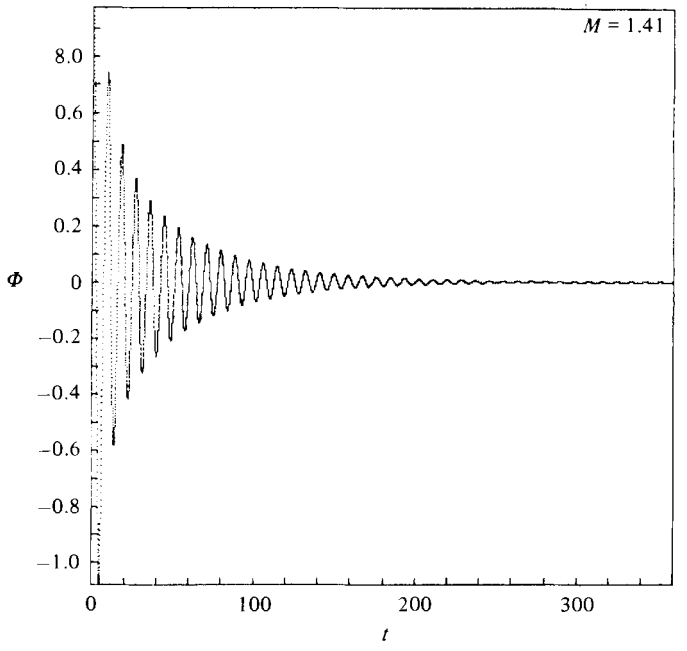

FIGURE 2. The evolution of the mode amplitude for 9000 iterations of the differential equations (59)–(62). $M = 1.41$ here, and amplitudes, which began at $\Phi(0) = E_{11}(0) = E_{20}(0) = 1.0$, $\phi(0) = 0.5$, and $R = 1.0$, settle into their fixed-point values.

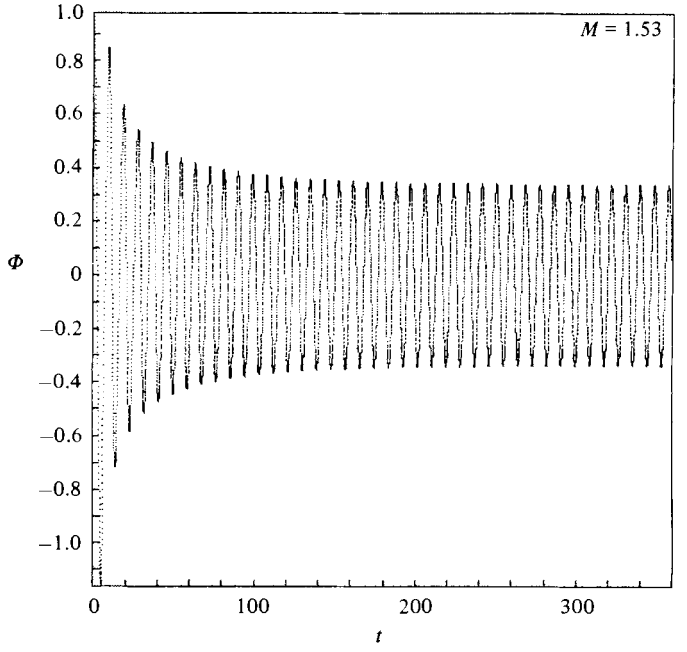

FIGURE 3. Same as figure 2 with $M = 1.53$. The fixed point has bifurcated into a limit cycle.

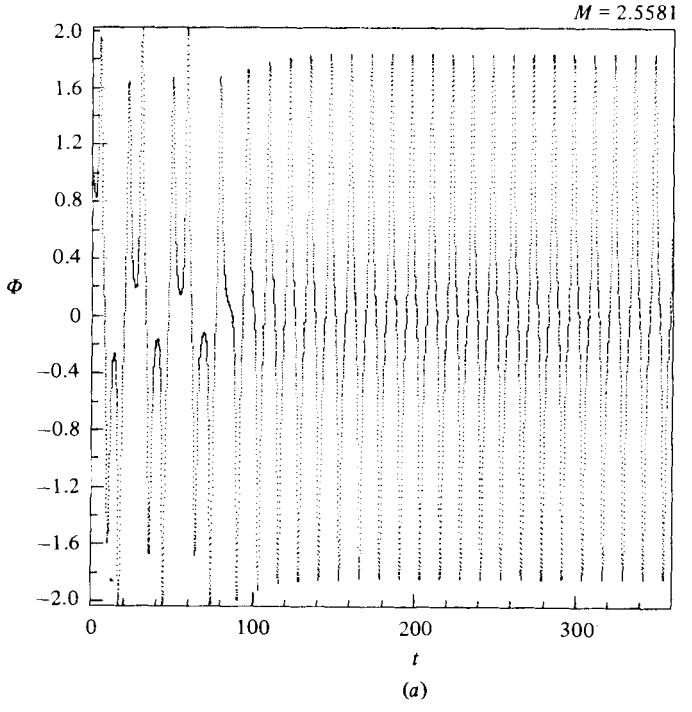

(*a*)

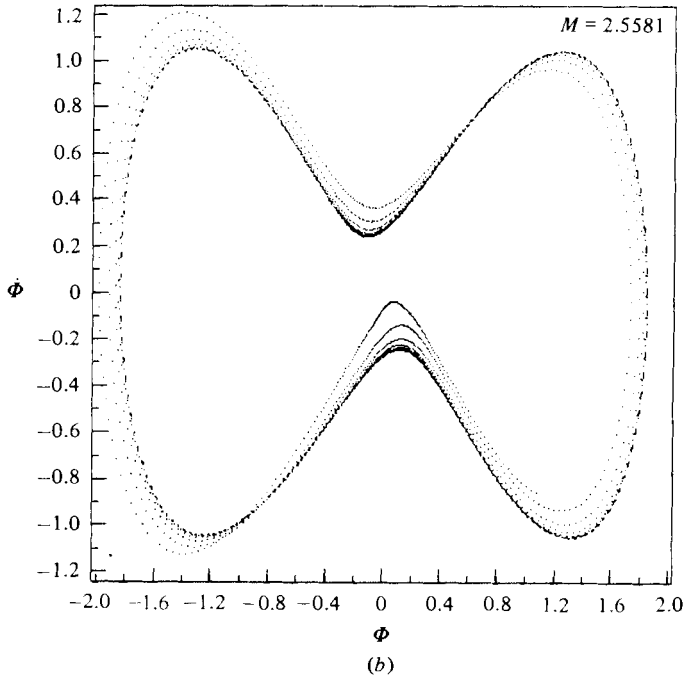

(*b*)

FIGURE 4. Same as figure 2 with $M = 2.5581$. In (*b*) is shown Φ versus $\dot{\Phi}$ for the last 7000 time steps.

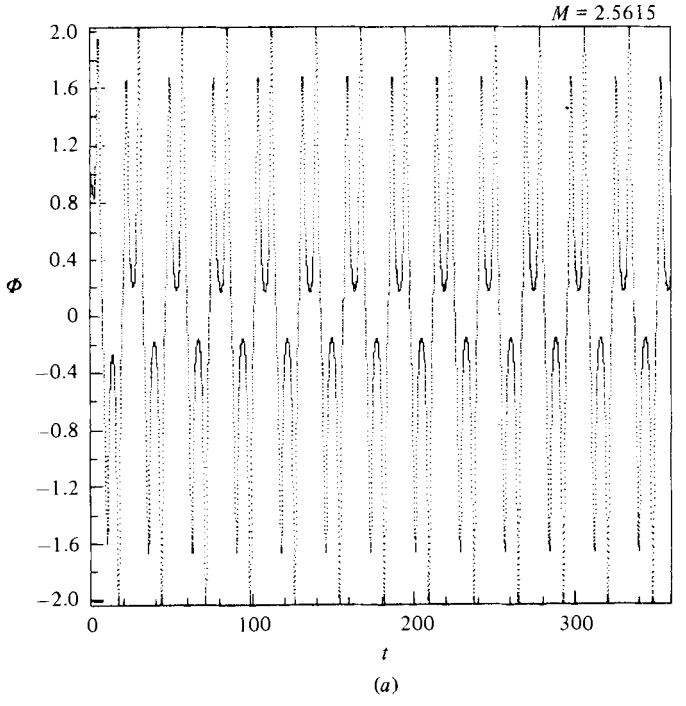

FIGURE 5. Same as figure 4 with $M = 2.5615$.

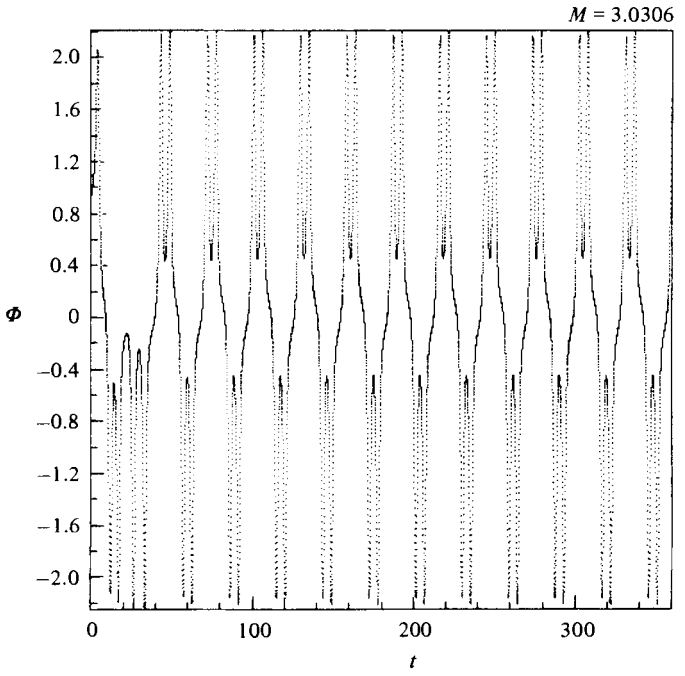

FIGURE 6. Same as figure 2 with $M = 3.0306$.

the results of our calculations at $M = 1.41$. We show only $\Phi(t)$. In the time series for the amplitude we exhibit 9000 points generated by a fourth-order Runge–Kutta scheme with fixed time steps. Figure 3 contains the same information at $M = 1.53$. In these and subsequent figures the initial values of our amplitudes were chosen to be $\Phi(0) = E_{11}(0) = E_{20}(0) = 1.0$ and $\theta(0) = 0.5$. For a range of other values for these initial conditions we have verified that the same asymptotic state is achieved after an initial transient.

For $1.5 \leqslant M < 2.5605$ the limit cycle is the stable attractor. In figure 4 we have the amplitude for $M = 2.5581$. In figure 4(*b*) only the last 7000 points on the orbit are shown. The transients show the near stability of a new stable attractor, but in each case the orbit settles down to the limit cycle as before. Choosing different initial conditions changes the details of the transient behaviour; the attractor is the same. By $M = 2.5615$, as displayed in figure 5, we see that the new attractor has become stable. In figure 5(*b*) for $\dot{\Phi}$ *vs.* Φ only the last 7000 points are displayed. The transition occurs at $M \approx 2.56051$ as we will discuss below.

We move on now, and in figure 6 we display our data at $M = 3.0306$, where we see an initial transient from yet another attractor setting in. This turns out to be the precursor to further transitions in the structure of the attractor which occur very near $M \approx 3.034063$.

In figure 7 we exhibit Φ and $\dot{\Phi}$ versus Φ for $M = 3.03535$. The non-periodic nature of the orbit is clear to the eye. We have examined this orbit in more detail by computing 10^4 and then 1.5×10^4 points on the orbit. We show in figure 8 the last 8500 points of $\dot{\Phi}$ versus Φ for 10^4 iterations, and, in figure 9, the last 13500 points of $\dot{\Phi}$ versus Φ for 1.5×10^4 iterations. Special attention should be given to the structure which is clearly growing up at this M. It is the projection of the non-periodic structure evolving in the four-dimensional phase space. We are going to refer to this as a strange

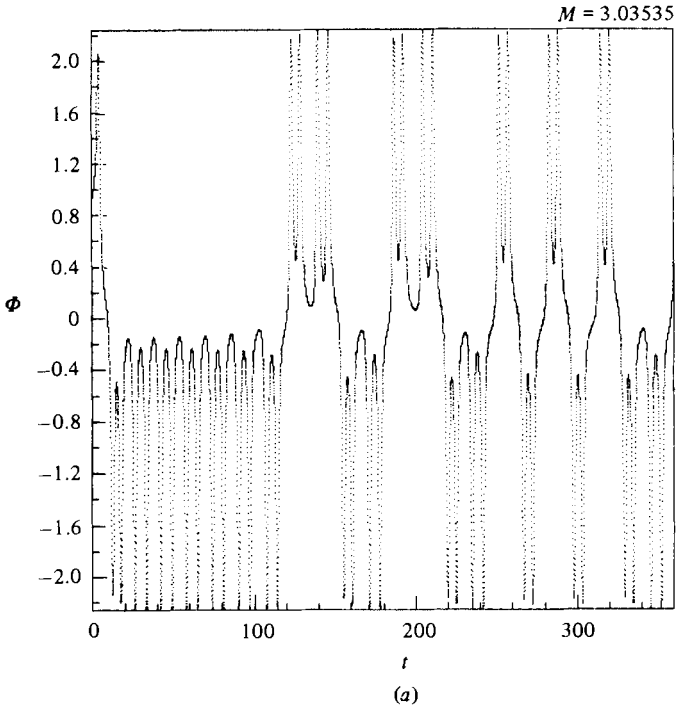

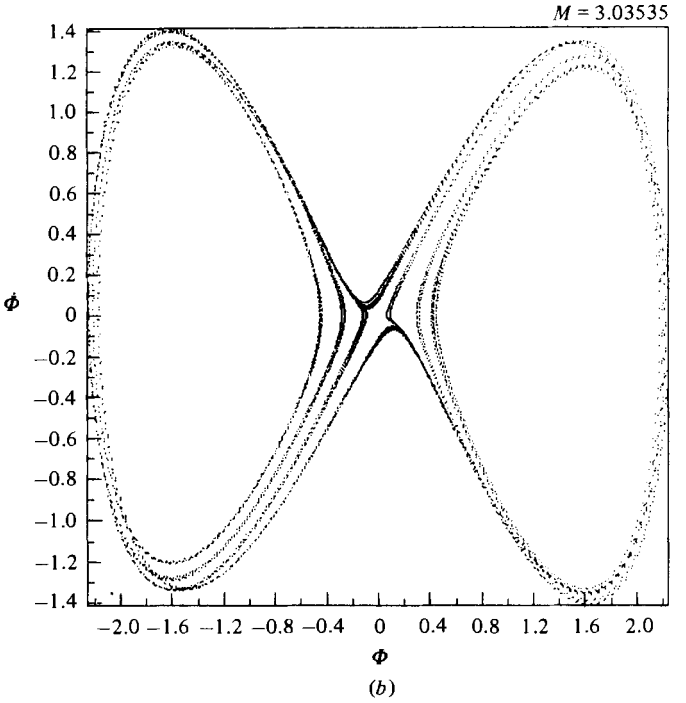

FIGURE 7. Same data as figure 4 with $M = 3.03535$, which has brought us to the regime of chaotic or non-periodic motion.

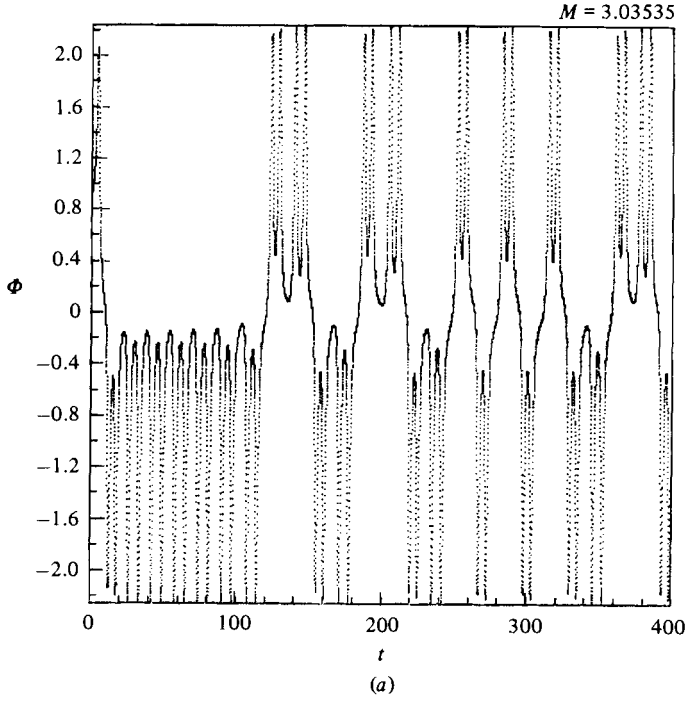

(a)

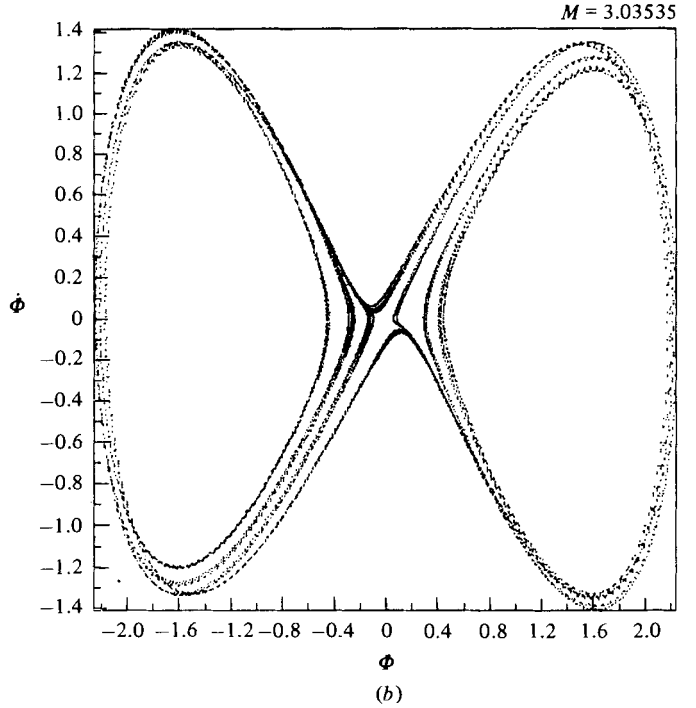

(b)

FIGURE 8. (a) $\Phi(t)$ for 10000 iterations of (59)–(62) at $M = 3.03535$. (b) $\dot{\Phi}$ versus ϕ for the last 8500 points in the orbit. Compare (b) with figure 7(d) and 9(b) to see the development of the strange attractor as it appears projected into the $(\dot{\Phi}, \Phi)$ plane.

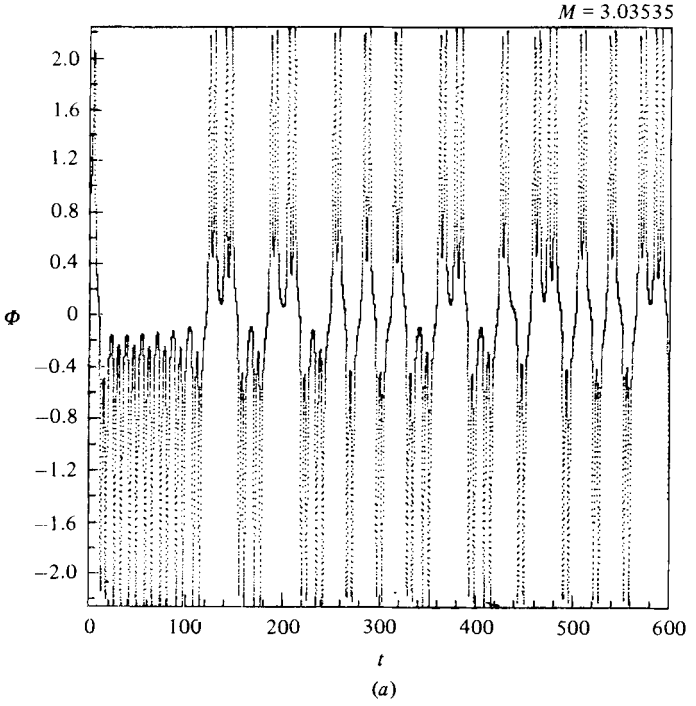

(*a*)

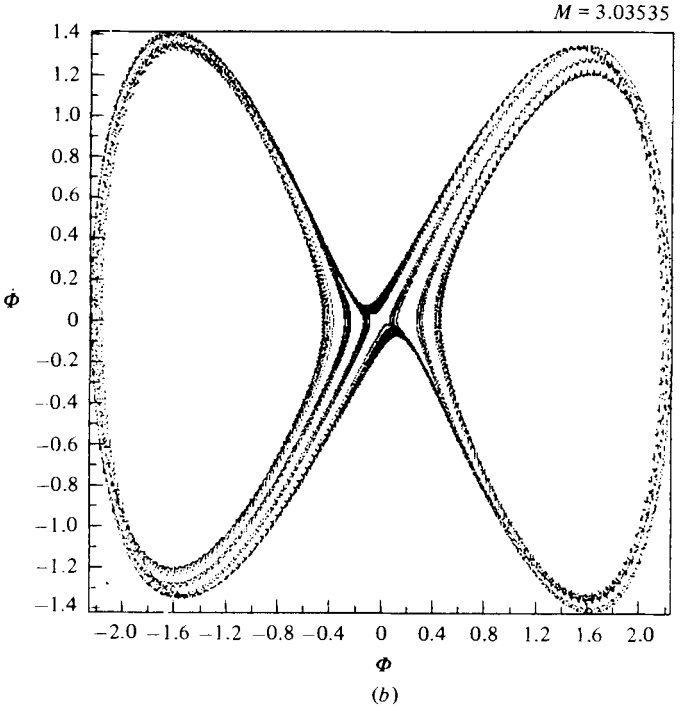

(*b*)

FIGURE 9. Same as figure 8 with 15000 points of $\Phi(t)$ in (*a*) and the last 13500 points of $\dot{\Phi}$ versus Φ in (*b*).

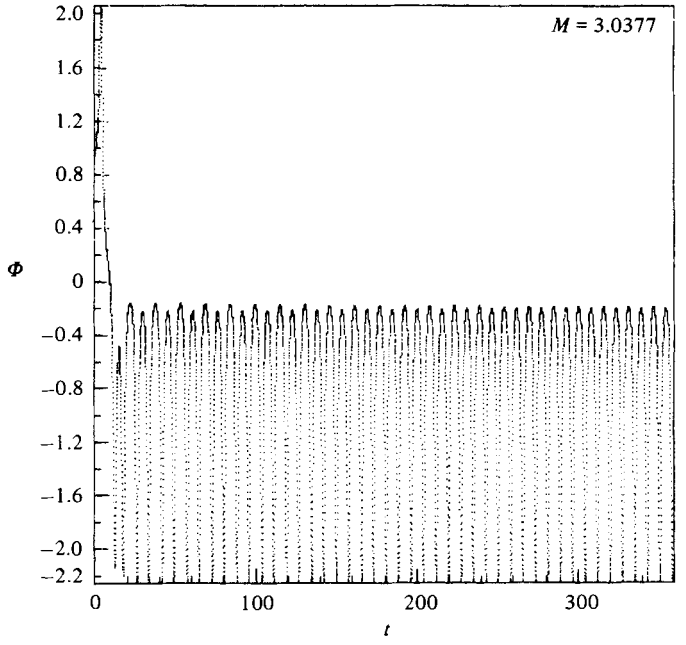

(a)

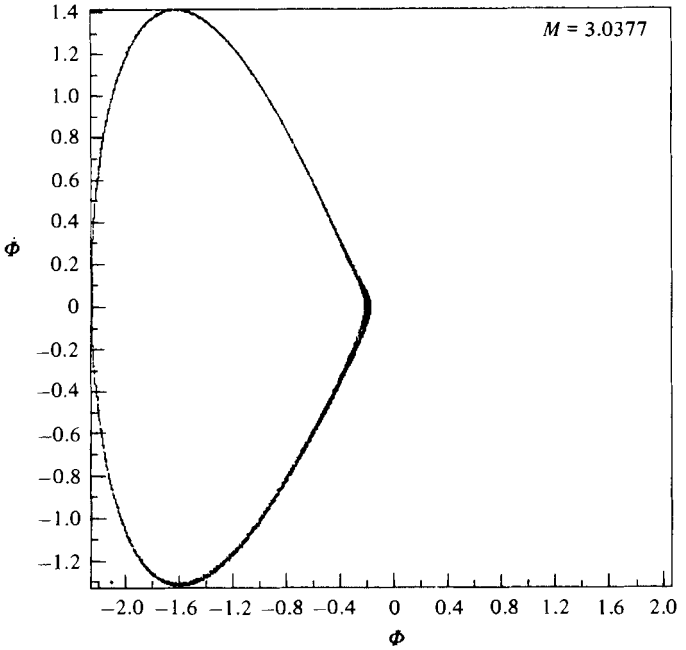

(b)

FIGURE 10. Same as figure 4 with $M = 3.0377$.

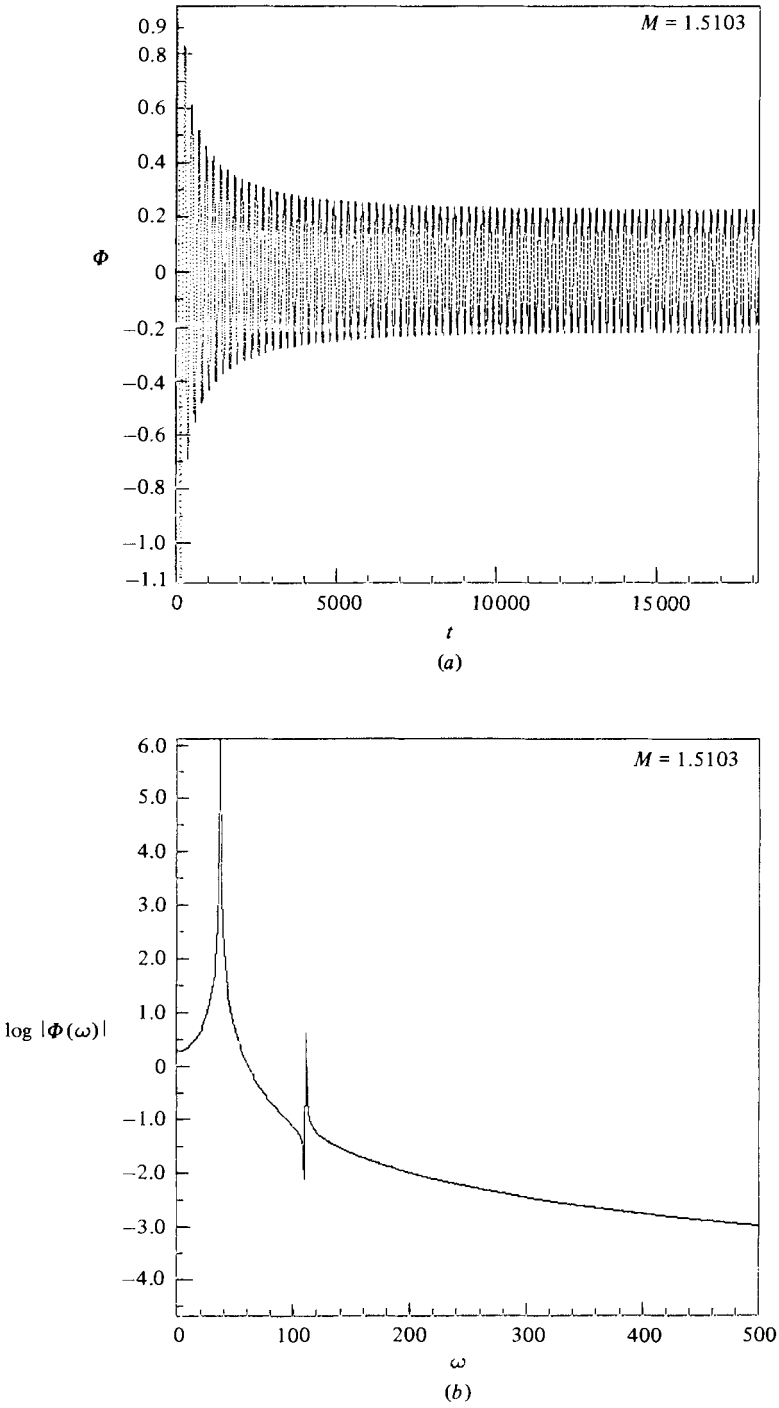

FIGURE 11. For $M = 1.5103$ we display in (a) $\Phi(t)$ for 18192 steps along the orbit. In (b) we plot $\log|\Phi(\omega)|$, the Fourier transform of the last $2^{13} = 8192$ steps along the orbit. Only the first 500 bins in frequency are shown; this takes us in ω up to $\omega = 9$. Beyond bin 500 is smooth noise. The bifurcation to a limit cycle occurs at a frequency of $\sqrt{\frac{1}{2}}$, which corresponds to bin 37 on this plot. That frequency and one harmonic are visible here.

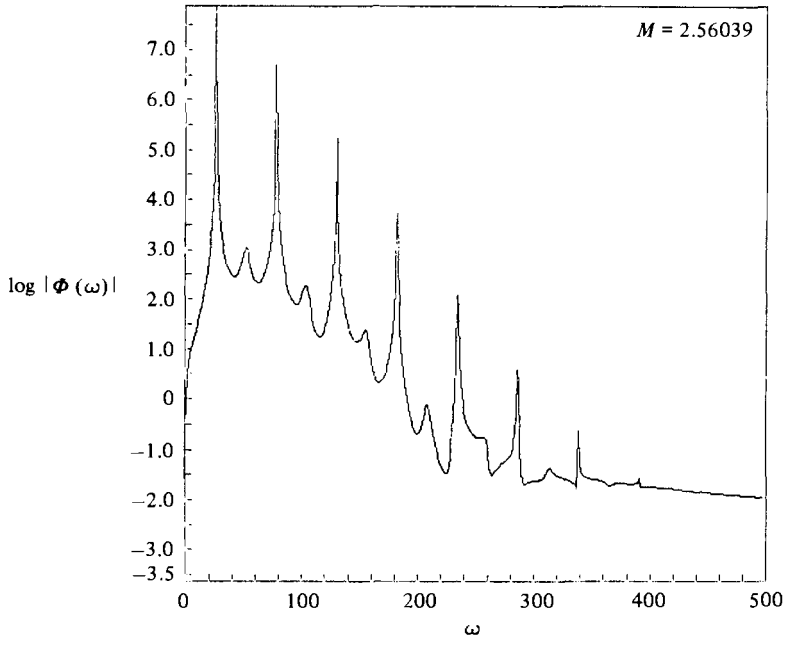

FIGURE 12. Same as figure 11 for $M = 2.56039$ for $\log|\Phi(\omega)|$. This is just below the value of M where the limit cycle becomes unstable.

attractor, though we have not verified that the curve occupies a non-integral volume. It is sufficient for our purposes that the behaviour is non-periodic.

The final time series we display is for $M = 3.0377$ in figure 10. The orbit has returned to a limit cycle. Indeed, for all $M > 3.037$ that we have examined, only a limit cycle was observed. We have non-exhaustively searched up to $M \approx 45$. It is interesting to note that the Lorenz equations (Lorenz 1963) derived from the Bénard convection problem also show a limit cycle for large Rayleigh number (Robbins 1979) – the analogue of our M.

Next we turn to the power spectra of the time series we have studied. Three issues are important here: (1) the frequency of the limit-cycle behaviour just as the fixed point has become unstable; (2) the appearance of new frequencies after bifurcation; and (3) the onset of broadband 'noise' when strange attractors are present.

We calculated our power spectra by solving the differential equations for $N = 18192 = 10^4 + 2^{13}$ equal time steps, $\Delta t = 0.04$. Then the last 2^{13} points were Fourier-transformed, and a subset of the Fourier coefficients are displayed.

At the onset of the limit cycle the frequency should be $(\gamma R/\alpha + \gamma)^{\frac{1}{2}} = \sqrt{\frac{1}{2}}$ with our parameter choice. This should appear as a peak in the Fourier coefficient $J = N\Delta t/2\pi\sqrt{2} = 37$. In figure 11, where $M = 1.5103$, we show the time series $\Phi(t)$ for N steps and the power spectrum $\log|\Phi(\omega)|$. Indeed the spectrum consists of the frequency we expect, plus harmonics.

Now when the limit cycle becomes unstable two 'generic' routes that can be taken are (1) a second Hopf bifurcation leading to a second independent frequency or (2) a period-doubling bifurcation leading to a fundamental at half the frequency. In figure 12 we show $\log|\Phi(\omega)|$ at $M = 2.56039$, which, as the orbit reveals, is very close to the bifurcation. The power spectrum consists of mode number $J = 27$ and its harmonics. Figure 13 contains the same data at $M = 2.56051$, where the fundamental

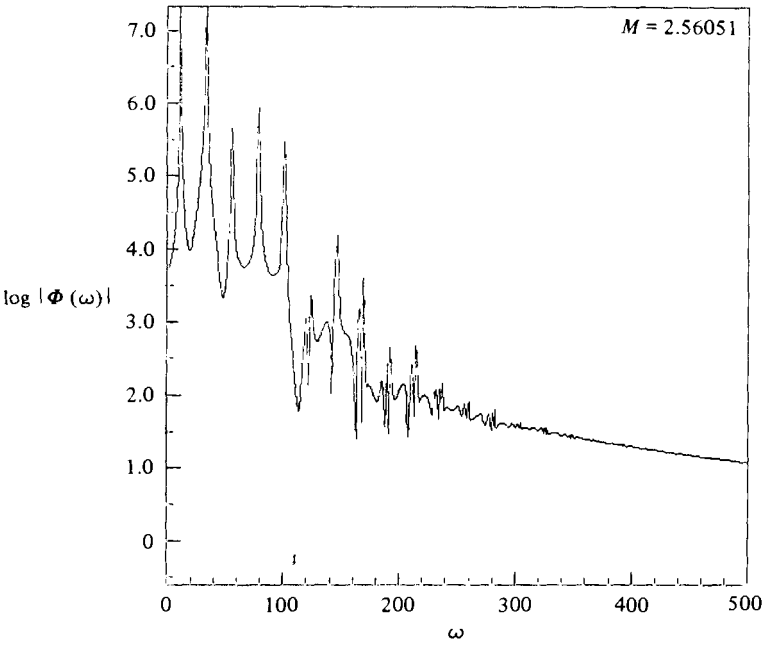

FIGURE 13. Same as figure 12 for $M = 2.56051$, which is just beyond the period doubling at $M = 2.56044$. Note that the fundamental here is half of the fundamental in figure 12.

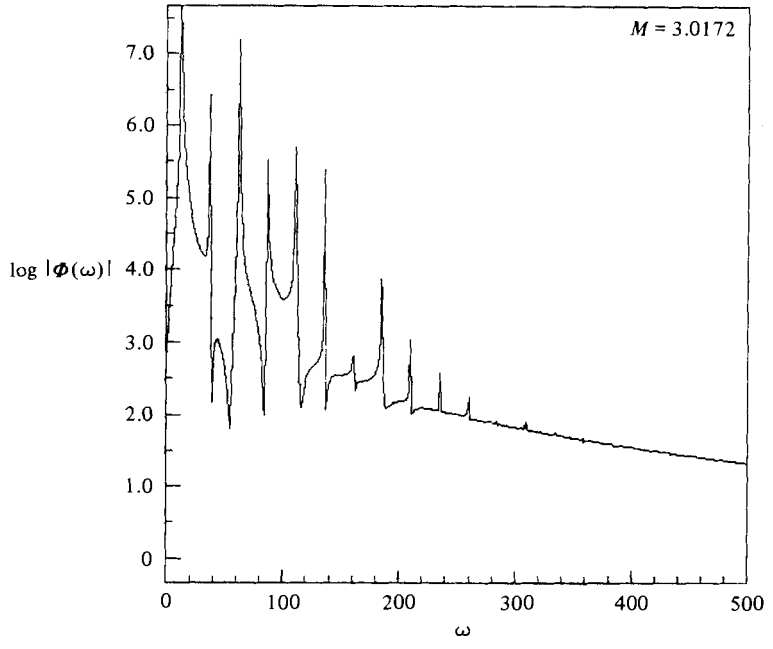

FIGURE 14. Same as figure 12 for $M = 3.0172$.

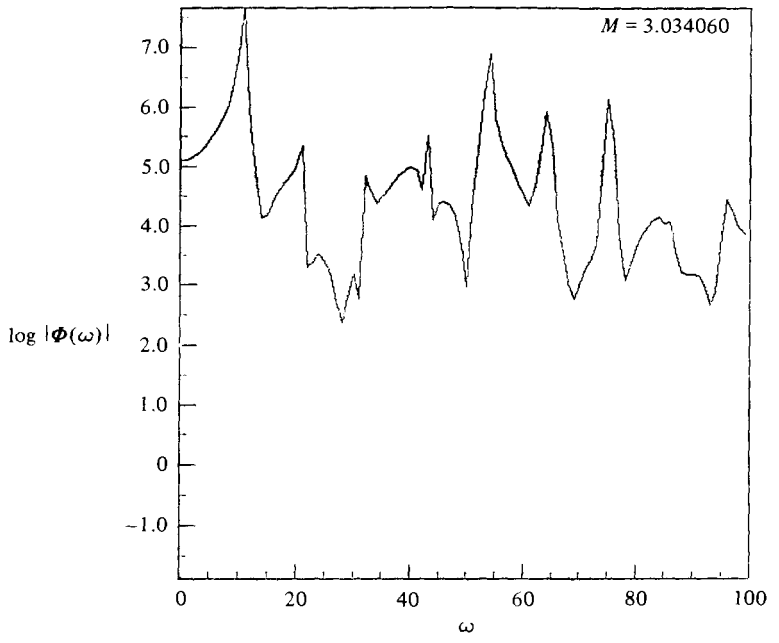

FIGURE 15. The power spectrum log $|\Phi(\omega)|$ for $M = 3.03406$, which is just before a second period doubling occurs. Only the first 100 bins out of 8192 are shown.

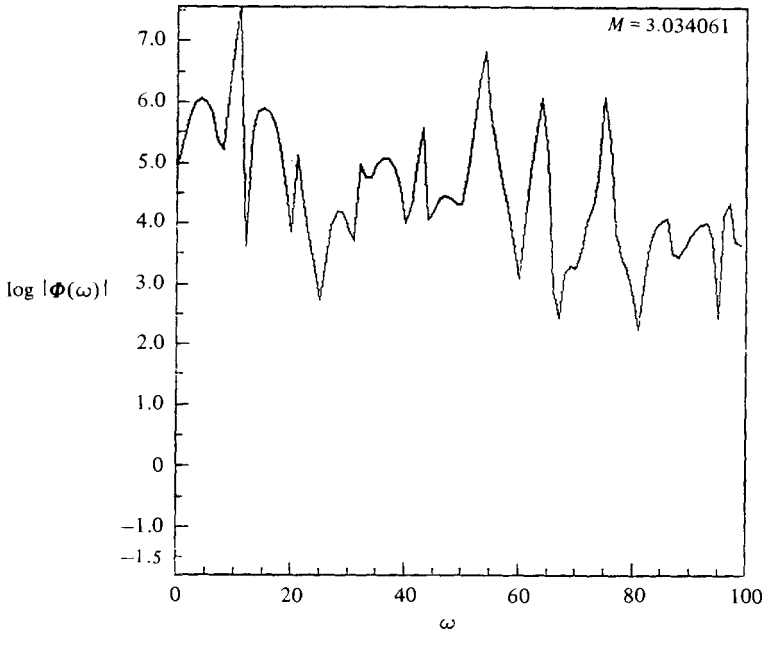

FIGURE 16. The power spectrum log $|\Phi(\omega)|$ for $M = 3.03461$, which is just beyond the second period doubling. Only the first 100 bins out of 8192 are shown.

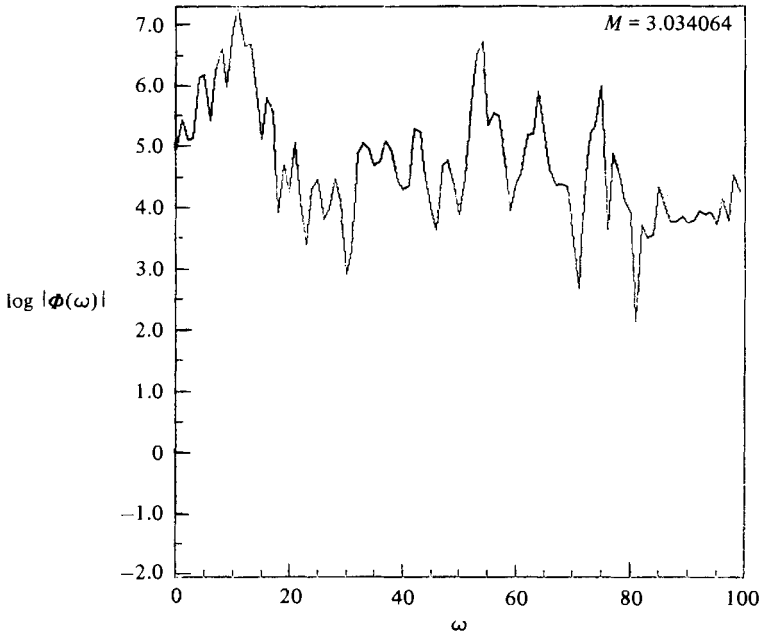

FIGURE 17. Same as figure 16 for $M = 3.034064$. Another period doubling is visible.

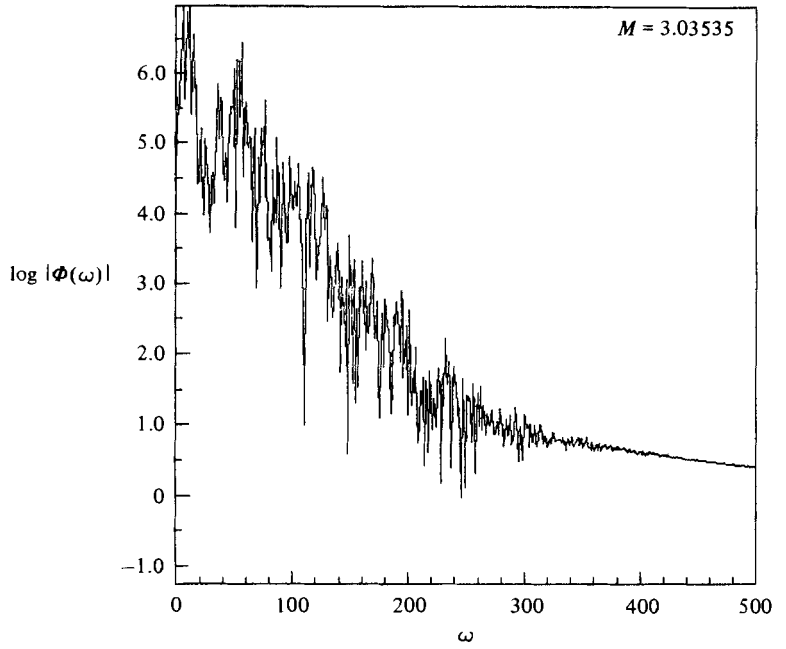

FIGURE 18. The power spectrum $\log|\Phi(\omega)|$ for $M = 3.03535$, which is in the chaotic regime. The broadband 'noise' is expected for the non-periodic behaviour on a strange attractor.

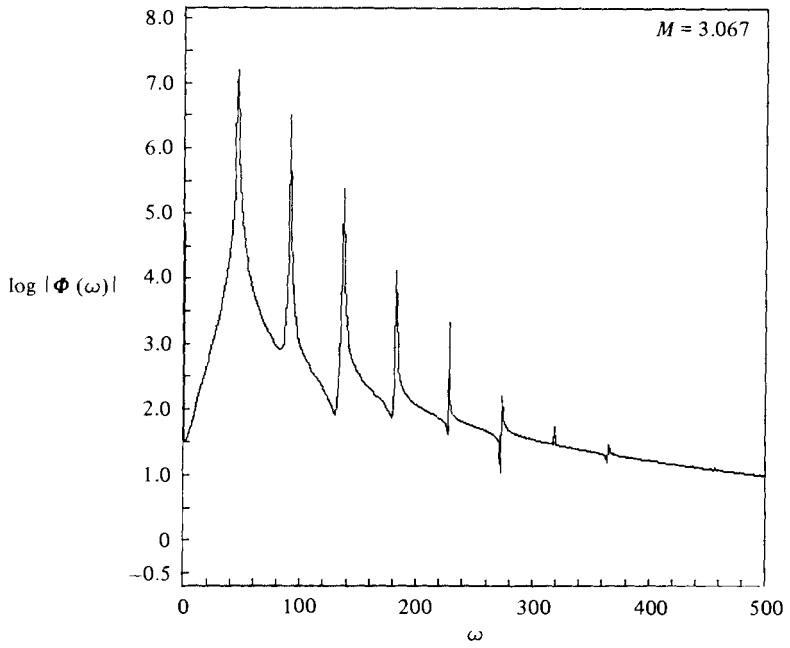

FIGURE 19. The power spectrum $\log|\Phi(\omega)|$ for $M = 3.067$, which is in the region $M > 3.037$ beyond which only a stable limit cycle is seen.

lies at $J = 12$. A careful survey of the power spectra in this interval reveals the period doubling to occur around $M = 2.56044$. From here to $M = 3.034$ we see in the power spectra only the new fundamental, which is a function of M, and its harmonics. Figure 14 at $M = 3.0172$ is typical.

The next interesting occurrences are at $M = 3.034$. In figure 15 we have $\log|\Phi(\omega)|$ for $M = 3.034060$, and figure 16 displays the same quantity for $M = 3.034061$. A second period doubling is now emerging. By $M = 3.034064$, shown in figure 17, yet another period doubling has occurred. Furthermore, we see at this point that the power spectrum has become 'broad' in the sense that there is power in a very large number of lines. At this stage we are also pushing the resolution of our numerical calculations of $\Phi(\omega)$.

Our last 'data' are at $M = 3.03535$ and $M = 3.067$. At the first value the plot in figure 18 of $\log|\Phi(\omega)|$ is the expected broadband 'noise' characteristic of non-periodic motion on a strange attractor. At $M = 3.067$ we have once again the clean spectrum consistent with a simple limit cycle.

4. Summary and outlook

In this paper we have analysed an oceanic internal gravity-wave field driven by energy sources at the surface. Our motivation in this work is the physical idea that the universal spectrum of Garrett & Munk is a steady state of the system with energy injection at long wavelengths and viscous dissipation at short scales. Further we argued that the statistical appearance of internal-wave measurements arises because the asymptotic attractor of the system is non-periodic or a strange attractor.

Our work in this note has concentrated on a specific model of driven internal-wave dynamics, and even then we have studied a truncated two-dimensional version of the

model for an ocean with constant buoyancy frequency. The truncation we used kept only the longest-wavelength modes and studied the nonlinear interaction among them. The numerical results reported in §3 show that, as a parameter which is proportional to the strength of forcing by the energy input mechanism is increased, the truncated system becomes unstable, develops a limit cycle via a normal Hopf bifurcation and then undergoes a sequence of period-doubling bifurcations to a strange attractor.

In the particular truncated model we analysed we found chaotic behaviour for a small parameter range, and, when the forcing became stronger yet, a regular limit cycle set in. The implication of this for oceanic internal waves is not that non-periodic behaviour results from only a small range of forcing strengths above which regular motion will be observed. Rather one should view our numerical work as an indication of what will be the fate of the larger number of modes which come into play when the forcing is increased. So we expect that, as soon as the forcing is raised above a (small) critical value, many modes will undergo the route to turbulent behaviour we have seen for a few modes.

Support for this view comes from the linear stability analysis of §2. Equation (29) gives the boundary of stability for our two-dimensional model. The critical forcing strength is proportional to viscosity (Γ_1 is dimensionless viscosity), as is the curvature of the critical $\mu_c(q, m)$ curve as a function of horizontal wavenumber $\pi m/L$ near the minimum of the curve. This means that for small viscosity, which is the actual case, the μ_c curve will have a broad minimum near $\mu \approx$ small. For small forcing, then, a broad band of modes will suffer the instabilities and undergo the sequence of bifurcations we have found. By our eventual choice of parameters in the numerical work reported we have, in effect, set $\Gamma_1 \approx 1$ by working on a viscous timescale. Our work shows the way in which the strange attractor 'unfolds'.

Our model for the driven internal-wave system introduced an energy-transfer field $E(\boldsymbol{x},t)$, which was held fixed on the oceanic surface and was carried through the medium by advection as well as being dissipated in the medium. An equally attractive model would add to the Navier–Stokes equation a body force $F(\boldsymbol{x}, t)\,\hat{\boldsymbol{z}}$ which contains a few frequencies reflecting the timescale of energy input through the surface into the internal-wave motion and a few wavenumbers reflecting the spatial distribution of the energy input. Each model tries to represent the surface driving of the oceanic internal gravity-wave field. Other sources of energy input (Thorpe 1975) can, of course, be modelled by additional distributed or localized forces.

It is a premise of the argument in this paper that the qualitative features of the chaotic or turbulent motion in the internal-wave system result from the presence of a strange attractor and are rather independent of the detailed nature of the energy sources. This premise is the underpinning of the specific model we analysed here: a few-mode truncation of a two-dimensional ocean with a uniform buoyancy frequency.

Our few-mode approximation keeps only the longest-wavelength degrees of freedom in the velocity, density and energy-transfer fields, It is perhaps surprising as well as gratifying that even in this severely truncated model we find stable limit cycles as well as chaotic, non-periodic attractors which act as if statistical. Details of the model aside – since clearly improvements of detail are called for – it does support our basic premise and invite extensive further investigation.

I wish to thank S. Flatté, G. Holloway and W. Munk for their valuable commentary on a draft of this work.

This work was supported by the Director, Office of Energy Research, Office of

Basic Energy Sciences, Engineering, Mathematics, and Geosciences Division, U.S. Department of Energy, under Contract DE-AC03-76SF00098, and DARPA Contract no. 4805-02.

Appendix

In this appendix we set up the three-dimensional version of our driven internal-wave-field model. Here we carry out and investigate certain features of the linear stability analysis.

Begin with the fundamental equations (1)–(4) from §2. In three dimensions there are four independent fields. We choose them to be the vertical velocity $u_3(\boldsymbol{x}, t)$, the vertical vorticity $\omega_3(\boldsymbol{x}, t)$, the variation of density $\rho_1(\boldsymbol{x}, t)$ about the mean stratification $\rho(x_3)$, and the variation of energy transfer $E_1(\boldsymbol{x}, t)$ about energy conduction. An equation for ω_3 comes from taking the curl of the momentum equation (1); our equation for u_3 comes from curling again. Then we have

$$\frac{\partial}{\partial t}\nabla^2 u_3 + f\frac{\partial \omega_3}{\partial x_3} + \nabla_\perp^2\left(\frac{g\rho_1}{\rho_0} + \beta E_1\right) = \nu\nabla^4 u_3 - \text{curl}\,(\text{curl}\,(\boldsymbol{u}\times\boldsymbol{\omega}))_3, \tag{A 1}$$

$$\frac{\partial \omega_3}{\partial t} - f\frac{\partial u_3}{\partial x_3} = \nu\nabla^2\omega_3 + \text{curl}\,(\boldsymbol{u}\times\boldsymbol{\omega})_3, \tag{A 2}$$

$$\frac{\partial \rho_1}{\partial t} + \boldsymbol{u}\cdot\boldsymbol{\nabla}\rho_1 = \frac{\rho_0 n^2}{g}u_3, \tag{A 3}$$

$$\frac{\partial E_1}{\partial t} + \boldsymbol{u}\cdot\boldsymbol{\nabla}E_1 + \frac{E_0}{D}u_3 = \kappa\nabla^2 E_1, \tag{A 4}$$

where $\boldsymbol{\nabla}_\perp = (\partial_1, \partial_2)$ is the horizontal gradient.

We perform scalings on these equations which are appropriate to the constant-n ocean. These scalings are the same as in §2 with the addition

$$(u_1, u_2, u_3) \to \mu n D(u_1, u_2, u_3), \tag{A 5}$$

$$(\omega_1, \omega_2, \omega_3) \to \mu n(\omega_1, \omega_2, \omega_3), \tag{A 6}$$

which replace the rescaling of the stream function.

After these rescalings we have

$$\frac{\partial}{\partial t}\nabla^2 u_3 + \frac{f}{n}\frac{\partial \omega_3}{\partial z} + \nabla_\perp^2(\rho_1 + E_1) = \Gamma_1\nabla^4 u_3 - \mu\,\text{curl curl}\,(\boldsymbol{u}\times\boldsymbol{\omega})_z, \tag{A 7}$$

$$\frac{\partial \omega_3}{\partial t} - \frac{f}{n}\frac{\partial u_3}{\partial z} = \Gamma_1\nabla^2\omega_3 + \mu\,\text{curl}\,(\boldsymbol{u}\times\boldsymbol{\omega})_z, \tag{A 8}$$

$$\left(\frac{\partial}{\partial t} + \mu\boldsymbol{u}\cdot\boldsymbol{\nabla}\right)\rho_1 = u_3, \tag{A 9}$$

$$\left(\frac{\partial}{\partial t} + m\boldsymbol{u}\cdot\boldsymbol{\nabla}\right)E_1 + \mu u_3 = \Gamma_2\nabla^2 E_1. \tag{A 10}$$

The linear stability of the trivial solution $u_3 = \omega_3 = \rho_1 = E_1 = 0$ is investigated by setting these fields equal to a single eigenmode of the linear system. With the boundary conditions $u_3 = 0$ at $z = 0, -1$; $\partial\omega_3/\partial z = 0$ at $z = 0, 1$; $u_1 = 0$ at $x = \pm L$; and $u_2 = 0$ at $y = \pm L$ we can express the eigenmodes in terms of sines and cosines.

Write

$$u_3 = \mathrm{i}\tilde{W}\,\mathrm{e}^{\mathrm{i}q\pi z}\,\mathrm{e}^{\mathrm{i}(\pi/L)(m_1 x+m_2 y)}\,\mathrm{e}^{\lambda t}, \tag{A 11}$$

$$\omega_3 = \tilde{\Omega}\,\mathrm{e}^{\mathrm{i}q\pi z}\,\mathrm{e}^{\mathrm{i}(\pi/L)(m_1 x+m_2 y)}\,\mathrm{e}^{\lambda t}, \tag{A 12}$$

$$\rho_1 = \mathrm{i}\tilde{\rho}\,\mathrm{e}^{\mathrm{i}q\pi z}\,\mathrm{e}^{\mathrm{i}(\pi/L)(m_1 x+m_2 y)}\,\mathrm{e}^{\lambda t}, \tag{A 13}$$

$$E_1 = \mathrm{i}\tilde{E}\,\mathrm{e}^{\mathrm{i}q\pi z}\,\mathrm{e}^{\mathrm{i}(\pi/L)(m_1 x+m_2 y)}\,\mathrm{e}^{\lambda t}. \tag{A 14}$$

This leads to a 4×4 matrix equation for the amplitudes $\tilde{W}$, $\tilde{\Omega}$, $\tilde{\rho}$ and $\tilde{E}$. A non-trivial solution requires the vanishing of

$$k_{qm}^2\lambda^4 + k_{qm}^4\lambda^3(2\Gamma_1+\Gamma_2) + \lambda^2\left[k_3^2\frac{f^2}{n^2} + k_\perp^2(1-\mu) + k_{qm}^4\Gamma_1(\Gamma_1+2\Gamma_2)\right.$$
$$\left. + \lambda k_{qm}^2\left[\Gamma_2\frac{k_3^2 f^2}{n^2} + k_{qm}^6\Gamma_1 + k_\perp^2 + \Gamma_1 k_\perp^2(1-\mu)\right] + \Gamma_1\Gamma_2 k_{qm}^4 k_\perp^2 = 0, \right. \tag{A 15}$$

where

$$k_3 = \pi q, \quad k_\perp^2 = \frac{\pi^2}{L^2}(m_1^2+m_2^2). \tag{A 16}$$

The detailed discussion of (A 15) would lead us far astray. We choose instead to consider an instructive special case: $\Gamma_1 = 0$.

If $\Gamma_1 = 0$, that means we are dealing with the inviscid limit of the internal-wave theory. One solution to (A 15) is $\lambda = 0$; the other values of λ satisfy

$$k_{qm}^2\lambda^3 + \Gamma_2 k_{qm}^4\lambda^2 + \lambda^2\left[k_3^2\frac{f^2}{n^2} + k_\perp^2(1-\mu)\right] + \Gamma_2 k_{qm}^2\left[\frac{k_3^2 f^2}{n^2} + k_\perp^2\right] = 0. \tag{A 17}$$

If the last term is non-zero, then there is always one negative real root of (A 17). The other roots have negative real parts until $\mu = 0$. For $\mu < 0$ the asymptotic motion of the internal wave field is $u_3 = \omega_3 = E_1 = \rho_1 = 0$; that is, the background state with no fluid motion. When $\mu = 0$ the system undergoes a Hopf bifurcation with frequency

$$\Omega(q,m)^2 = \left[\frac{f^2k_3^2 + k_\perp^2 n^2}{k_{qm}^2}\right]\frac{1}{n^2}; \tag{A 18}$$

that is, the usual linear internal-wave frequency. The amplitude of the motion is proportional to $\mu^{\frac{1}{2}}$.

In this inviscid limit even the smallest forcing sets all modes q, m into motion. So a finite-mode approximation won't do. The excitation of modes is then solely governed by the total energy available and is essentially independent of the nonlinear dynamics. The motion would be quasi-periodic. The spectrum would show peaks at all modal values permitted by energy conservation rather than a broad background characteristic of 'statistical' behaviour.

REFERENCES

Arnol'd, V. I. 1978 *Mathematical Methods of Classical Mechanics*, §16. Springer.

Bretherton, F. P. 1969 Waves and turbulence in stably stratified fluids. *Radio Sci.* **4**, fR 1279.

Chandrasekhar, S. 1961 *Hydrodynamic and Hydromagnetic Stability*, §103. Oxford University Press.

Eckmann, J.-P. 1981 Roads to turbulence in dissipative dynamical systems. *Rev. Mod. Phys.* **53**, 643.

Eriksen, C. C. 1978 Measurements and models of fine structure, internal gravity waves, and wave breaking in the deep ocean. *J. Geophys. Res.* **83**, 2989.

Fenstermacher, P. R., Swinney, H. L. & Gollub, J. P. 1979 Dynamic instabilities and the transition to chaotic Taylor vortex flow. *J. Fluid Mech.* **94**, 103.

GARRETT, C. C. & MUNK, W. 1975 Space time scales of internal waves: a progress report. *J. Geophys. Res.* **80**, 291.

GARRETT, C. C. & MUNK, W. 1979 Internal waves in the ocean. *Ann. Rev. Fluid Mech.* **11**, 339.

HOLLOWAY, G. 1980 Oceanic internal waves are not weak waves. *J. Phys. Oceanogr.* **10**, 906.

IOOSS, G. & JOSEPH, D. 1981 *Elementary Stability and Bifurcation Theory*. Springer.

KURAMOTO, Y. & KOGA, S. 1982 Anomalous period doubling bifurcations leading to chemical turbulence. *Phys. Lett.* **92A**, 1.

LANFORD, O. E. 1980 Turbulence and strange attractors. In *Hydrodynamic Instabilities and the Transition to Turbulence* (ed. H. L. Swinney & J. P. Gollub). Springer.

LIBCHABER, A. & MAURER, J. 1981 A Raleigh–Bénard experiment: helium in a small box. *Ecole Normale Preprint.*

LORENZ, E. N. 1963 Deterministic nonperiodic flow. *J. Atmos. Sci.* **20**, 130.

LYUBIMOV, D. V. & ZAKS, M. A. 1983 On two mechanisms of the transition to chaos in finite dimensional models of convection. *Preprint of the Perm State University, USSR.*

OTT, E. 1981 Strange attractors and chaotic motions of dynamical systems. *Rev. Mod. Phys.* **53**, 655.

PEDLOSKY, J. 1979 *Geophysical Fluid Dynamics*. Springer.

PHILLIPS, O. M. 1977 *The Dynamics of the Upper Ocean*, 2nd edn. Cambridge University Press.

ROBBINS, K. A. 1979 Periodic solutions and bifurcation structure at high R in the Lorenz model. *SIAM J. Appl. Maths* **36**, 457.

RUELLE, D. & TAKENS, F. 1971 On the nature of turbulence. *Commun. Math. Phys.* **20**, 167.

THORPE, S. A. 1975 The excitation, dissipation, and interaction of internal waves in the deep ocean. *J. Geophys. Res.* **80**, 328.

WATSON, K., WEST, B. J. & COHEN, B. J. 1976 Coupling of surface and internal gravity waves: a mode coupling model. *J. Fluid Mech.* **77**, 185.

WUNSCH, C. 1975 Deep ocean internal waves: what do we really know? *J. Geophys. Res.* **80**, 339.